Effect of Nozzle Clogging on Surface Flow and Vortex Formation in the Continuous Casting Mold

Continuous casting is used to manufacture more than 90% of steel in the world,[1] so understanding and optimizing the process is important to minimize defects in steel. Most of the defects affecting slab quality are associated with surface flow in the mold.[2] Asymmetric surface flow in the mold is one of the main phenomena attributed to cause inclusion entrainment,[3–6] which can make "sliver" defects in the rolled product, caused by inclusions being trapped in the solidifying shell in the mold.

Nozzle clogging is one of the severe problems that can induce asymmetric flow. The nozzle flow pattern can be changed by asymmetric flow through clogged regions, resulting in asymmetric flow in the mold. Asymmetric mold flow can cause faster surface flow on one side of the mold, causing level fluctuations, vortices[7–9] and instability of the interfacial layer between the molten steel and liquid mold flux.[10] These phenomena can entrain liquid mold flux into the molten steel, inducing entrapment of inclusions into the solidifying steel shell. On the other hand, slow surface flow can be induced on the opposite side, which results in abnormal low and non-uniform temperature, inducing non-uniform liquid mold flux layer thickness and serious problems during initial solidification.

Previous researchers have studied the causes and effects of nozzle clogging in continuous casting. Rackers and Thomas classified the types of clogs

as: agglomeration of deoxidation products, solid steel build-up, agglomeration of complex oxides and reaction product buildup; and the types of transport mechanisms of oxidation products to the nozzle wall as: turbulent recirculation zones, turbulent flow, rough nozzle wall and external corners.[11] Several researchers studied clogging detection[12] and clogging prevention.[13] Bai and Thomas investigated the effects of clogging near the slidegate on nozzle flow, and found that clogging affects both flow pattern and pressure drop.[14] Recently, Zhang, et al. evaluated the nozzle port clogging on inclusion removal, slag entrainment, heat transfer and the prediction of breakouts.[15]

This work investigates the effect of nozzle clogging on fluid flow in the nozzle and mold using $1/3$-scale water model experiments and computational modeling of the water model. Many previous successful studies of mold fluid flow have been done using water models[16–18] and computational modeling.[19–20] The current study applies water model experiments to quantify surface flow, vortex formation frequency, and computational modeling to explain the nozzle and mold flow pattern.

Methodology

Water Model Experiments —

Experiments were performed using a $1/3$-scale water model of the real continuous casting process, shown in Figure 1. The model consists of a tundish,

Abstract

Nozzle clogging induces asymmetric surface flow, causing vortex formation and inclusion defects. This work applies computational and experimental approaches. The resulting increase in the asymmetries of the surface flow velocities, velocity time variations and vortex occurrence frequency on opposite sides of the mold are quantified.

Authors

Seong-Mook Cho (top left) and Seon-Hyo Kim (top center), Pohang University of Science and Technology, Department of Materials Science and Engineering, Pohang, Republic of Korea (y104401@postech.ac.kr); Rajneesh Chaudhary (top right), ABB Corporate Research Center, Bangalore, India (rajneesh.chaudhary@gmail.com)

Brian G. Thomas (middle left), University of Illinois at Urbana-Champaign, Department of Mechanical Science and Engineering, Urbana, Ill., USA (bgthomas@uiuc.edu); Ho-Jung Shin (middle center), Korea Institute of Industrial Technology, Center for Resources Information and Management, Seoul, Republic of Korea (ceraby@kncpc@re.kr); Wung-Yuel Choi (middle right), operational technology development team, steelmaking department, Gwangyang Works, POSCO, Junnam, Republic of Korea (missko@posco.com)

Sung-Kwang Kim (bottom right), steelmaking technology development group, Gwangyang Works, POSCO, Junnam, Republic of Korea (sungkwang@posco.com)

Figure 1
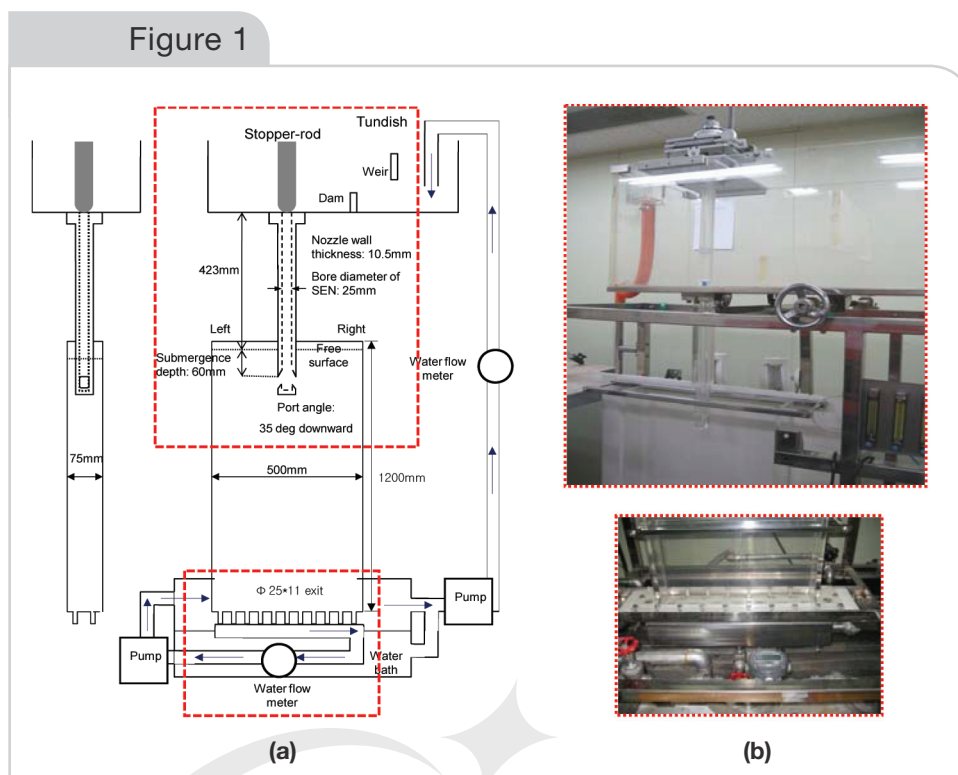
Schematic (a) and pictures (b) of $^1/_3$-scale water model.

stopper rod, submerged entry nozzle (SEN) and mold. Vertical movement of the stopper rod controls the water flowrate from the tundish through the SEN into the mold, by changing the size of the annular gap between the stopper end and the bottom of the tundish where it curves into the SEN. Water exits holes in the bottom of the mold to a holding water bath and is pumped continuously back up to the tundish.

Single-phase flow was adopted, so the possible effects of argon gas-bubble injection were not studied. The three nozzles were adopted for investigating the nozzle-clogging effects on surface flow and vortex formation, as shown in Figure 2. These nozzles have typical bifurcated, 35° down-angled rectangular ports with a 6.5-mm-deep well. Clogged nozzles have the cross-sectional areas of their left ports decreased by 33% (small-clog case) and 67% (severe-clog case), relative to the non-clogged right port. Further details

are given in Table 1. Table 2 provides details of the casting conditions, nozzle and mold dimensions of this $^1/_3$-scale water model and real caster. Similarity between the $^1/_3$-scale water model and the real caster conditions was determined based on maintaining a constant Froude number defined as the ratio of inertia force to gravitational force, $V/\sqrt{gL}$.

Surface velocity measurements were performed using electromagnetic current sensor located at the five positions shown in Figure 3; $^1/_2$L, $^1/_4$L positions on each side (L: distance across the mold width from the narrow face to SEN center) and the center position (in the gap between SEN outer wall and wide face). The sensor was dipped at the above positions from the free surface to measure instantaneous velocity signal at 10 mm below free surface. Instantaneous surface velocity data were collected for 1,000 seconds at a collecting frequency of 1 Hz with 1 Hz of response time.

Figure 2
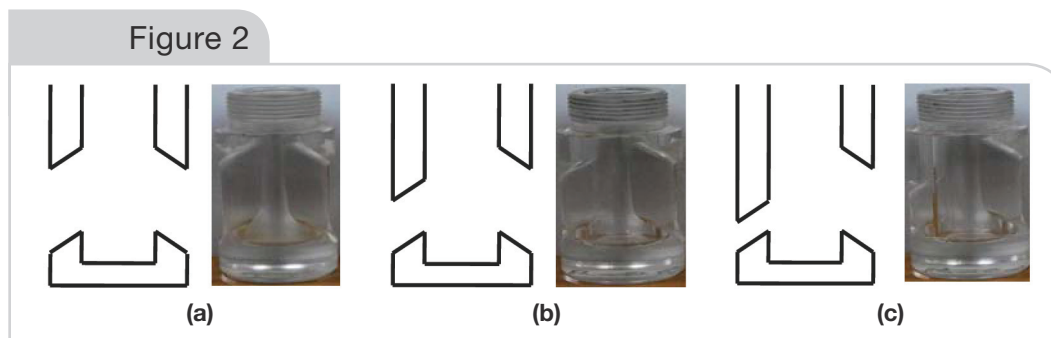
Nozzle of (a) no-clog case, (b) small-clog case and (c) severe-clog case.

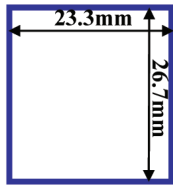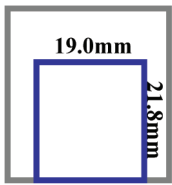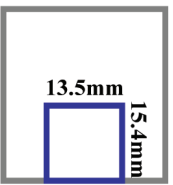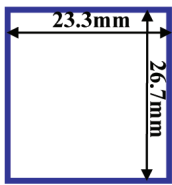## Table 1

Dimensions of Nozzle Ports

	Left port		Right port
No-clog	Small-clog	Severe-clog	All cases

No-clog: 23.3mm × 26.7mm
Small-clog: 19.0mm × 21.8mm
Severe-clog: 13.5mm × 15.4mm
All cases (Right port): 23.3mm × 26.7mm

Table 2

Processing Conditions for Experimental and Computational Works

	1/3-scale water model	Real caster
Casting speed	0.917 m/minute	1.59 m/minute
Water flowrate	34.4 LPM	537 LPM (3.77 tons/minute)
Mold width	500 mm	1,500 mm
Mold thickness	75 mm	225 mm
SEN depth	60 mm	180 mm
ρ_{fluid}	998.2 kg/m^3 (water)	7,020 kg/m^3 (steel)
μ_{fluid}	0.001003 kg/m-s (water)	0.0067 kg/m-s (steel)
Nozzle (well-bottom type) port angle	35°	
Nozzle ports	No-clog: symmetric ports Small-clog: 0.67 asymmetric left port Severe-clog: 0.33 asymmetric left port	
Nozzle bore diameter (inner/outer)	25 mm/46 mm	75 mm/138 mm
Shell	No	Yes
Gas injection	No	Yes

Figure 3

(a)   **(b)**
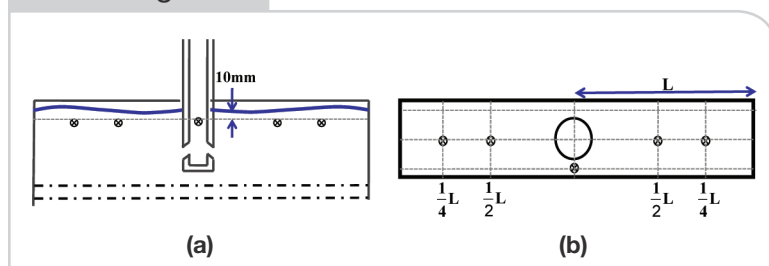
Locations of electromagnetic current sensor for measuring velocity.

The sensor has a circular cylinder head with 8 mm diameter and 20 mm height, which can measure surface velocity, including in the small gap between the SEN and mold, as shown in Figure 4. Two components of horizontal surface velocity are measured, one parallel and one perpendicular to the mold width direction. Flow direction angle and velocity magnitude are determined from the velocity components, to quantify the surface flow vector.

To investigate nozzle clogging effects on vortex formation, sesame seeds were used as tracer particles for visualization and vortex phenomena were recorded with a video camera. Vortices were observed in four regions near the SEN, as shown in Figure 5. After recording, the number and location of all vortices lasting over two rotations were counted from the recorded video. The number of vortices in each region was divided by total measuring time (10 minutes) to calculate the local "frequency" of vortex formation.

Computational Modeling — A three-dimensional finite-volume computational model was applied to investigate the flow pattern in a nozzle and mold for the no-clog, small-clog and severe-clog cases. The
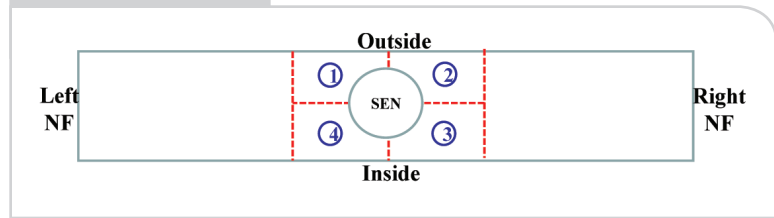
Figure 4
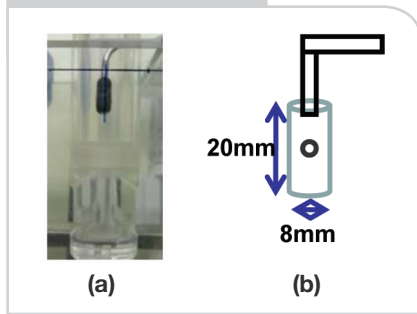
Picture (a) and schematic (b) of electromagnetic current sensor.

Figure 5

Regions where vortex formation was observed and counted.

steady-state, incompressible, Navier-Stokes equations with standard k-ε model have been solved in the commercial computational fluid dynamics (CFD) package program, FLUENT, to simulate the time-averaged turbulent flow. To decrease computer efforts, one-quarter nozzle and mold domains were used to simulate flow for the no-clog case (4-fold symmetry) and half domains were used for the small- and severe-clog cases (2-fold symmetry), as shown in Figure 6. Hexahedral cells were used for structured meshing of each domain; 107,356 cells with the no-clog case, 206,304 cells with the small-clog case and 202,610 cells with the severe-clog case.

To obtain more accurate simulations of fluid flow in the mold, the SEN domain was connected with the mold domain and calculated together.[15] For inlet boundary conditions where flow enters the sides of a cylinder representing part of the tundish bottom, the normal velocity was applied to match the flowrate in the $^1/_3$-scale water model, along with 10^{-5} m^2/second^2 for turbulent kinetic energy and 10^{-5} m^2/second^3 for

turbulent kinetic energy dissipation rate. At the mold bottom, outlet boundary conditions of 0 pascal of gauge pressure, 10^{-5} m^2/second^2 for turbulent kinetic energy and 10^{-5} m^2/second^3 for dissipation rate were applied. The top surface of the mold was a stationary wall with 0 pascal shear stress components for free-slip boundary condition. For all three cases, convergence of solving the equations was defined when all scaled residuals were stably reduced below 10^{-4}.

Nozzle Flow

To investigate the effects of nozzle port clogging on nozzle flow, velocity magnitude contours and streamlines are presented in Figure 7 for the three cases. The two clog cases have "small" clogging with the left port 33% smaller than the right port and "severe" clogging with the left port 67% smaller. The asymmetric port size causes asymmetric flow through the ports. The small-clog case has only 48% of the total flowrate exiting through the clogged left port. Severe clogging is much more asymmetric, with only 25% of the flowrate exiting through the clogged left port. Furthermore, higher velocity is induced through the non-clogged port, which causes higher momentum flow toward the right side of the mold. The backflow usually observed at the top of these oversized ports is not found in the clogged left port, which has low flowrate, low velocity and a more uniform velocity profile.

Table 3 shows the jet characteristics leaving each nozzle port. As expected, increasing asymmetry of the port sizes causes increased asymmetry of jet velocity, jet angle, turbulent kinetic energy and turbulent kinetic dissipation rate. The vertical jet angle becomes larger (directed more steeply downward) at the non-clogged port and smaller at the clogged port, relative to the average vertical jet angle with no clogging. The difference in vertical jet angle between the left and right port increases from 5.2° in the small-clog case to 6.9° in the severe-clog case. Average jet force is calculated by multiplying the flowrate and average jet speed. Total jet force from both ports increases

Figure 6
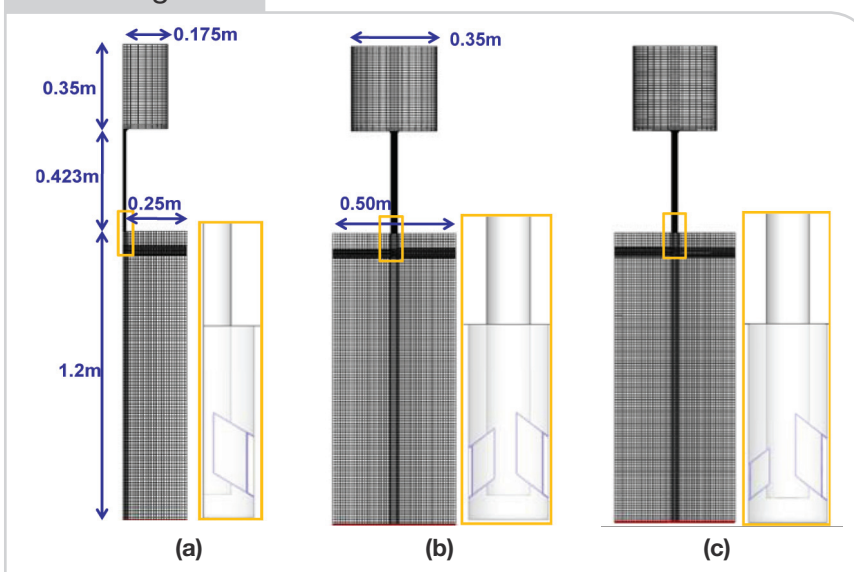
Domains and meshes of nozzle and mold with (a) no, (b) small and (c) severe clogging.

Figure 7
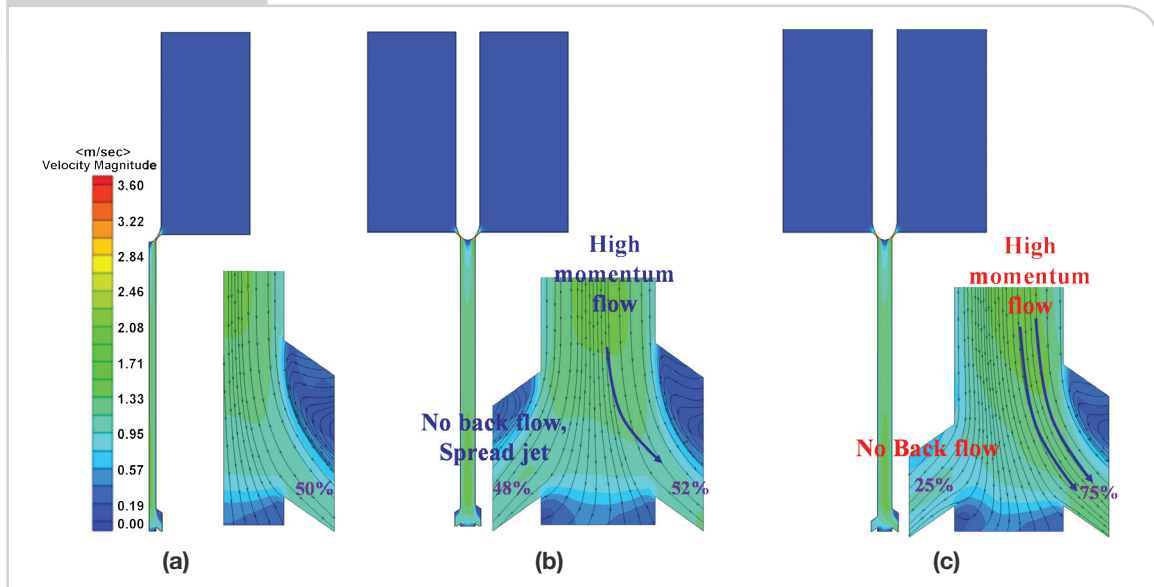
Flow pattern in the SEN with (a) no, (b) small and (c) severe clogging.

Table 3

Jet Characteristics

|	No-clog		Small-clog		Severe-clog	
	Left	**Right**	**Left**	**Right**	**Left**	**Right**
Weighted average nozzle port velocity in x-direction (outward) (m/second)	0.450	0.450	0.568	0.550	0.542	0.636
Weighted average nozzle port velocity in y-direction (horizontal) (m/second)	0.042	0.042	0.017	0.009	0.022	0.015
Weighted average nozzle port velocity in z-direction (downward) (m/second)	0.315	0.315	0.343	0.404	0.327	0.497
Vertical jet angle (degree)	−35.0	−35.0	−31.2	−36.4	−31.1	−38.0
Horizontal jet angle (degree)	0	0	0	0	0	0
Average jet speed (m/second)	0.55	0.55	0.66	0.68	0.63	0.81
Flowrate (kg/second)	0.286 (50%)	0.286 (50%)	0.276 (48%)	0.296 (52%)	0.145 (25%)	0.427 (75%)
Averaged jet force (N)	0.157	0.157	0.182	0.201	0.091	0.346
Maximum velocity magnitude (m/second)	0.98	0.98	1.10	1.17	0.87	1.28
Weighted average turbulent kinetic energy (m^2/second^2)	0.022	0.022	0.043	0.020	0.033	0.019
Weighted average turbulent kinetic energy dissipation rate (m^2/second^3)	0.782	0.782	2.12	0.797	1.47	0.731
Backflow zone (%)	17.2	17.2	0	16.9	0	17.2

with nozzle clogging. Asymmetry of jet force between the left and right ports increases with more clogging, from 12% difference with small clogging to 58% difference with severe clogging.

Mold Flow Pattern

Asymmetric jet flow from the nozzle due to partial clogging of one port induces asymmetry of the mold flow pattern, causing an unbalanced double roll pattern, as shown in Figure 8. With clogged nozzles, strong surface flow from the right narrow face crosses sides to suppress the uprising flow from the left narrow face. This decreases the size of the upper circulation region at the left side, where the port is partly clogged. In the severe-clog case, the flow does not rise upward after hitting the left narrow face, due to

Figure 8
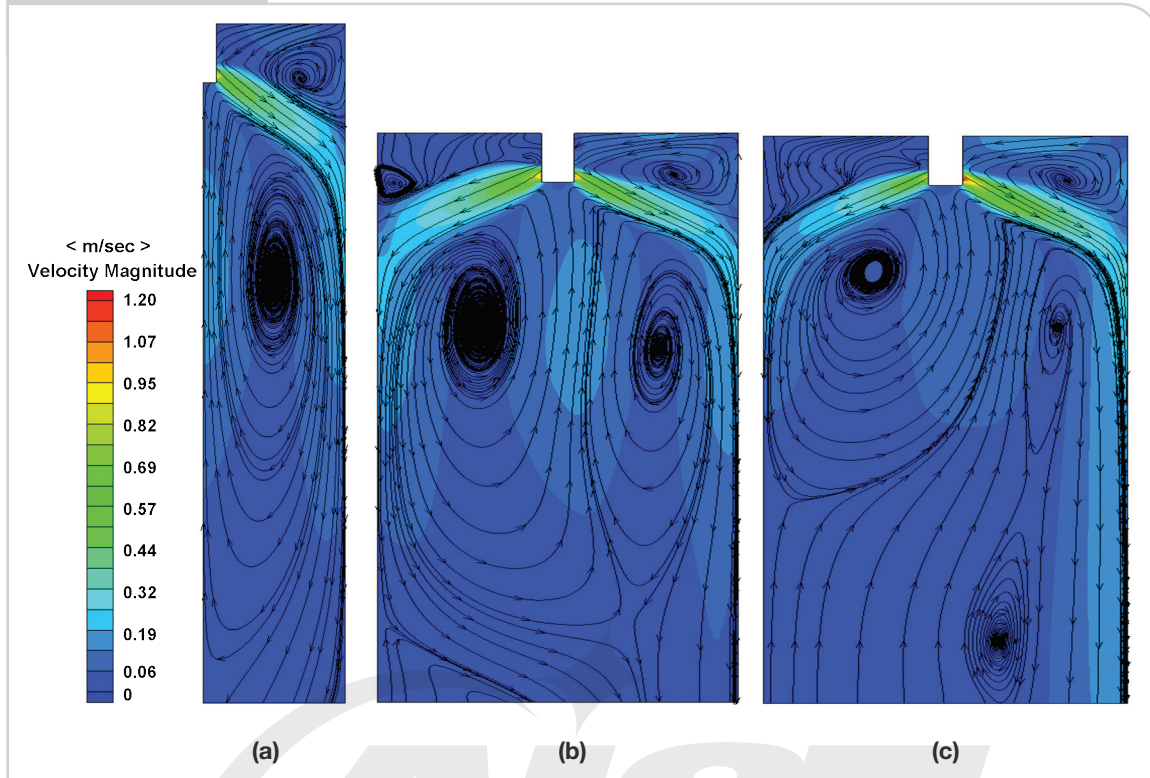
Flow pattern in the SEN with (a) no-, (b) small- and (c) severe-clog case.

the high strength of this cross-flow coming from the other side. The faster flow from the non-clogged side, in this severe-clog case, generates strong upward and downward flows after hitting the right narrow face. The strong upward flow can be detrimental in shearing off liquid slag from the top surface. The strong downward flow can be detrimental by taking inclusions deep into the mold cavity along the right narrow face, inducing more internal defects. This imbalanced flow behavior in the mold is consistent with the nozzle flow, explained with the help of jet angle and jet force in the previous section.
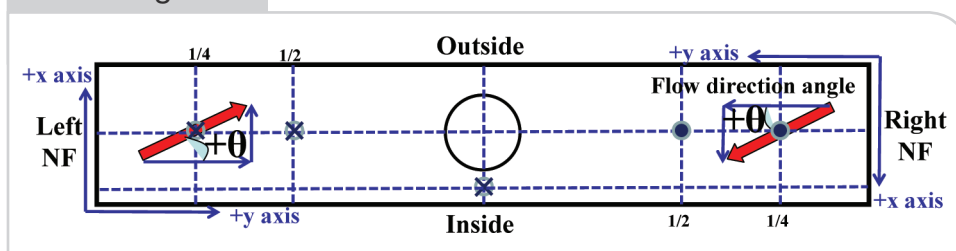
Surface Flow Velocity

To investigate nozzle-clogging effects on instantaneous surface flow, the electromagnetic current sensor is used to measure the two horizontal components of instantaneous surface velocity at five places on the surface of the mold as a function of time. Flow direction angle, θ, as defined in Figure 9, is determined by arctangent calculation from two velocity components. Note that the coordinate axis definition for this calculation changes between mold sides.

The unbalanced mold flow pattern induces asymmetric surface flow, as shown in Figures 10 and 11. Each graph shows the time variation of the velocity magnitude (black lines) and direction angle (blue lines) of the surface flow. Figure 10 sequentially shows the results at the $^1/_4$ width location from the left narrow face, $^1/_2$ width location from left narrow face, $^1/_2$ width location from right narrow face and $^1/_4$ width location from right narrow face (NF). Results in the gap between the SEN outer wall and mold inner wall are shown in Figure 11.
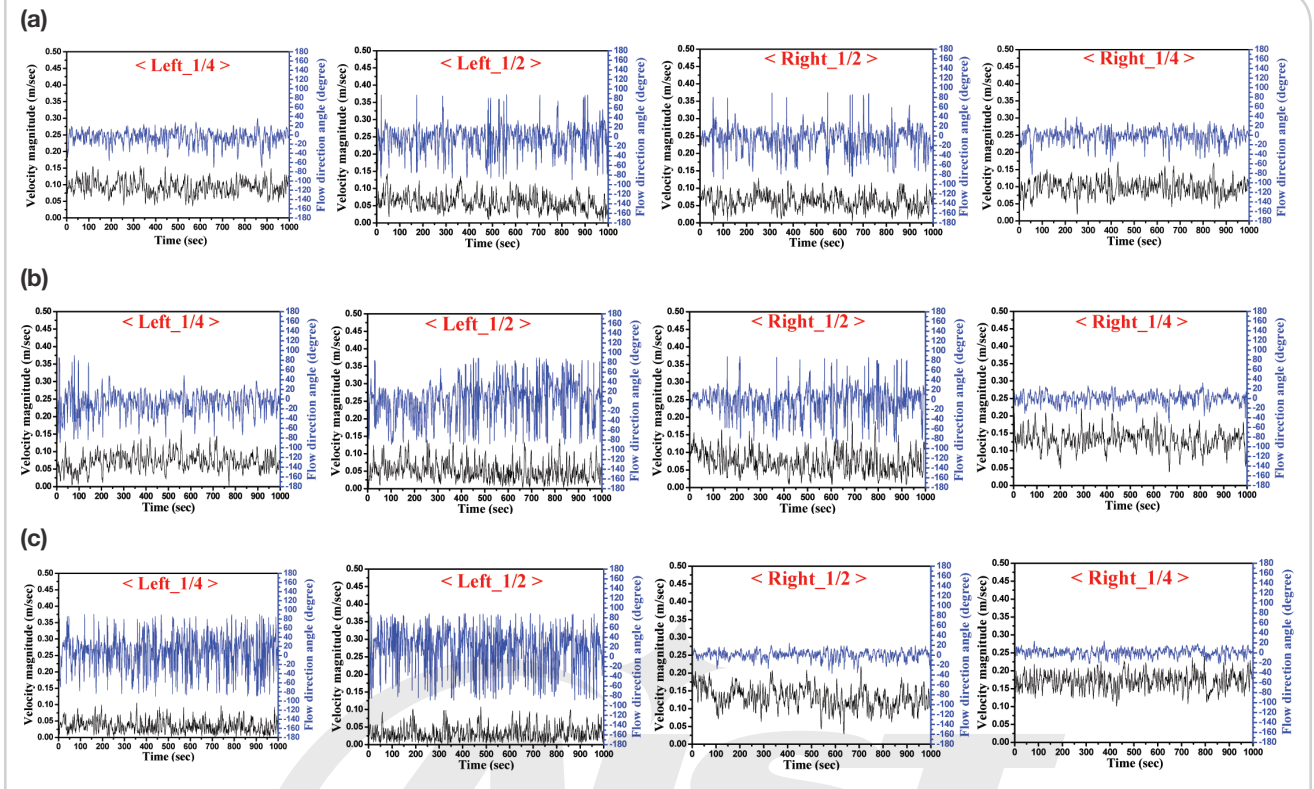
Surface flow becomes slower and more chaotic toward the SEN in both sides with a non-clogged nozzle. This trend of velocity magnitude and direction
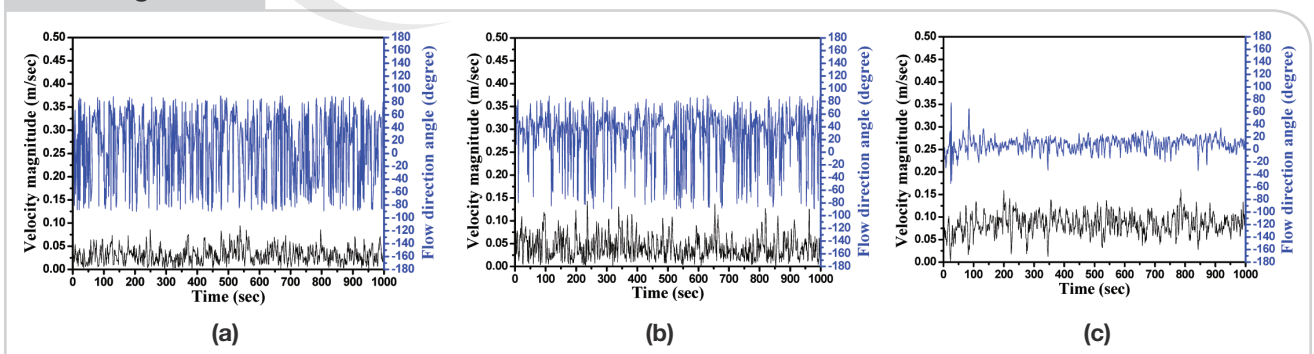
Figure 9

Definition of flow direction angle on both sides of SEN.

Figure 10

Instantaneous velocity histories at the four different surface positions across the mold width with (a) no-clog, (b) small-clog and (c) severe-clog cases.

Figure 11

Instantaneous velocity histories through the surface center (gap between SEN and mold) with (a) no-clog, (b) small-clog and (c) severe-clog cases.

angle of surface flow is the same with clog cases. Nozzle clogging makes faster and more consistent surface flow from the right NF same side with non-clogged port than the left NF same side with clogged port. The faster surface flow is caused by more force of jet flow from the non-clogged port, which results in faster uprising flow after impinging at the narrow face. On the other side, surface flow at the left (slower) side is more chaotic than the right side, showing the large fluctuation of flow direction angle, and this trend is severe with more clogging. More

asymmetrical flow between the left and right sides makes the flow faster in the gap between the SEN and the mold. In a clogged nozzle, the flow in the gap has a more consistent direction angle with higher velocity.

Figure 12 shows the time-average flow pattern, including the measured velocity vectors and magnitudes (top) and calculated speed contours and streamlines (bottom). As shown in the instantaneous velocity histories in Figures 10 and 11, nozzle clogging causes asymmetry of the average surface flow in the mold. Flow at the right (non-clogged) side is faster

Figure 12
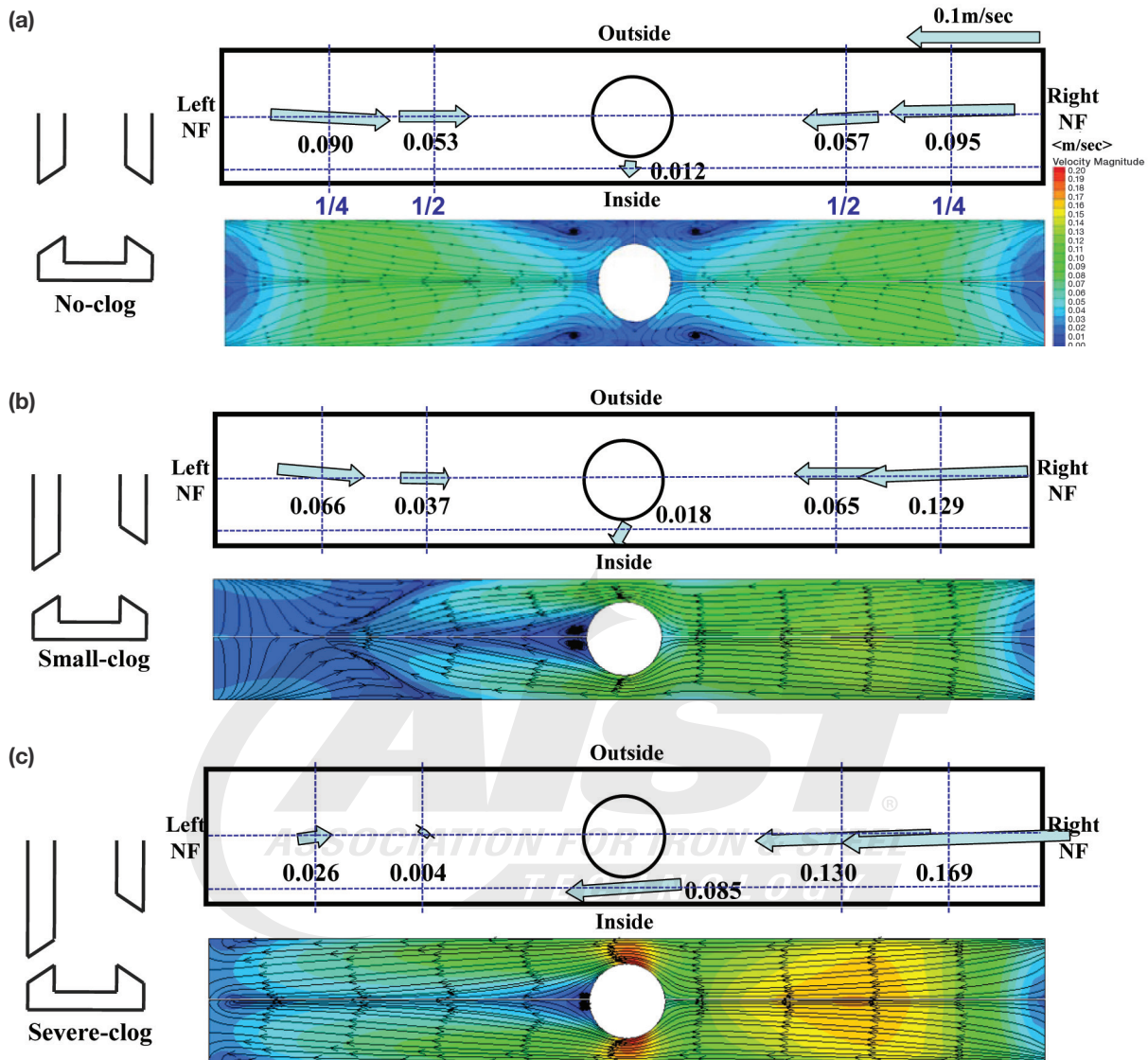
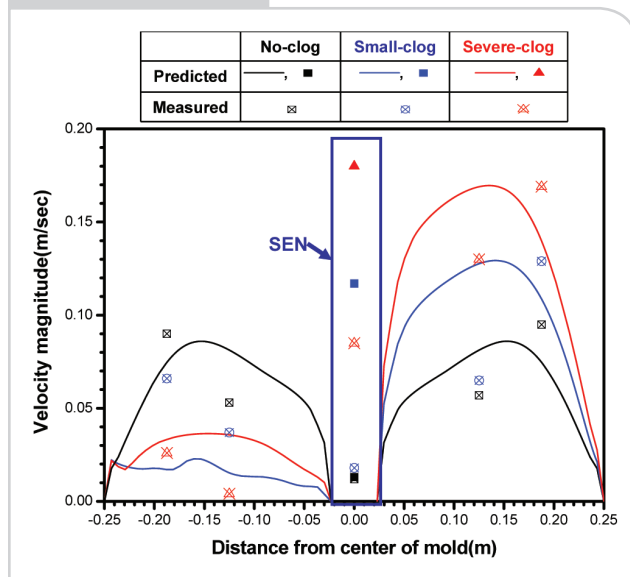Surface flow in the mold with (a) no-, (b) small- and (c) severe-clogged nozzle.

than the left (clogged port) side, causing more flow toward the left narrow face, and faster flow in the gap between SEN and mold. With no clogging, flow in the gap is directed toward the wide face, as the surface flows impinge from both sides. This is quite realistic and physically consistent since its asymmetry and normal velocity should be zero. With a clogged left port, the stronger surface flow from the right side overcomes flow from the left side. This causes consistent flow through the gap toward the left side with clogging.

The measured and predicted surface flow directions differ at the left side of the mold. In the small-clog case, the flow direction at $1/2L$ position of the left side is predicted toward the left narrow face. Surface flow direction with the severe-clog case is totally

directed toward the left side. This overprediction of the severity of the surface asymmetry is caused by a slight overprediction of the $1/2L$ surface velocity on the right side, and the corresponding extra momentum that suppresses the left side flows more than measured. As shown in Figure 13, the surface velocity is predicted to be greatest at the $1/2L$ location, but the measurements are greatest at the $1/4L$ location. These differences between simulations and measurements are likely due to the inability of this simple steady-state turbulence model to capture the complex transient vortexing flow.

In spite of this overprediction of surface flow asymmetries between right and left, the predictions match reasonably well with the measurements of surface velocity, as shown in Figure 13. Nozzle clogging clearly

Figure 13

Comparison of velocity magnitude between measurements and computational modeling.

induces strong asymmetric surface flow in the mold. Surface flow at the side of the mold with the non-clogged port is faster than the clogged-port side. More flow asymmetry between left and right sides induces faster flow in the gap between SEN and mold.

Vortex Formation

Almost all vortices form within 60 mm from the mold center in the four regions defined in Figure 5. Vortices at the first and third regions rotate counter-clockwise, and rotate clockwise at the second and fourth regions, as shown in Figure 14. The number printed in each of the four regions is the vortex formation frequency, calculated by counting how many vortices formed during 10 minutes. As expected, nozzle clogging causes asymmetric vortex formation with more vortices at the left side of the SEN. This is caused by more consistent and faster flow toward the left side through the gap between the SEN outer wall and the mold inner wall. In addition, more chaotic and slower flow at the $1/2$L location could be induced by vortex formation near the SEN. Thus, variations of flow direction angle are more severe with increased clogging at the $1/2$L location due to the increased vortices.

The frequency of occurrence of vortices in the left (first and fourth) regions is added and compared with the vortex frequency in the right (second and third) regions in Figure 15a and Table 4 to show the effect of left-right asymmetric flow caused by nozzle clogging. As expected, significant asymmetry is observed in the clog cases having asymmetric nozzle port sizes, and more severe with more clogging. Similarly, the vortex formation frequencies in the inside (third and fourth) regions are added and compared with the vortex frequency in the outside (first and second)

Figure 14
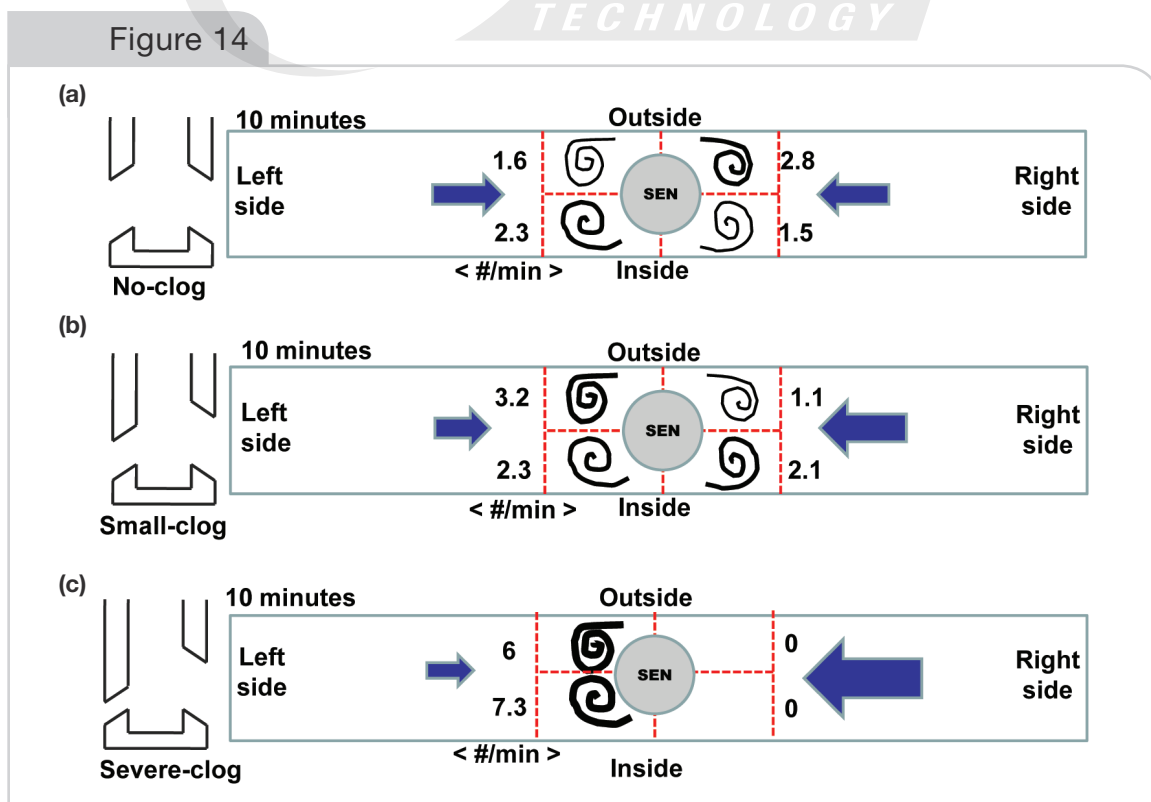
Vortex formation frequency in the mold with (a) no-clog, (b) small-clog and (c) severe-clog nozzle.

Figure 15
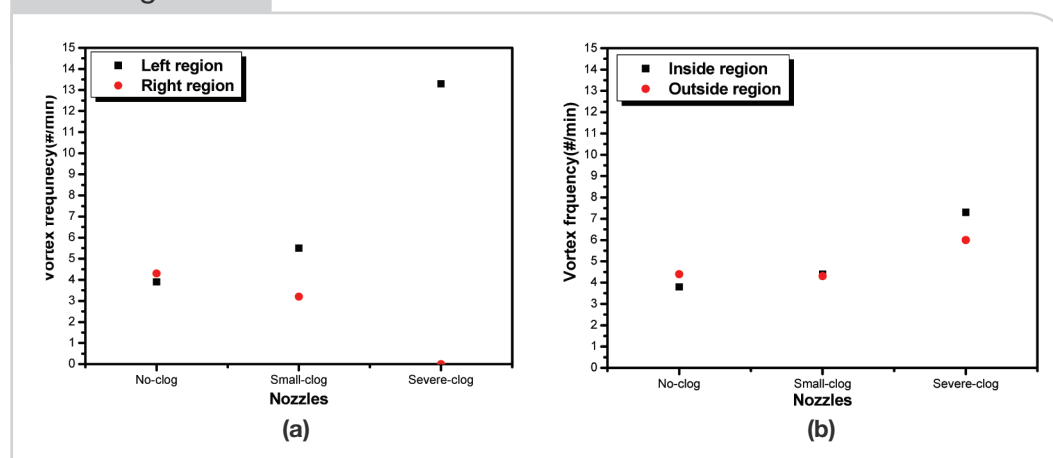
Vortex frequency comparing (a) left and right region and (b) inside and outside region.

Table 4

Comparison of Vortex Frequency Between Left and Right Regions

Vortex frequency (#/minute)	Left	Right	Total
No-clog	3.9 (48%)	4.3 (52%)	8.2
Small-clog	5.5 (63%)	3.2 (37%)	8.7
Severe-clog	13.3 (100%)	0	13.3

Table 5

Comparison of Vortex Frequency Between Inside and Outside Regions

Vortex frequency (#/minute)	No-clog	Small-clog	Severe-clog
Outside	4.4 (54%)	4.3 (49%)	6 (45%)
Inside	3.8 (46%)	4.4 (51%)	7.3 (55%)
Total	8.2	8.7	13.3

regions in Figure 15b and Table 5 to show the effect of asymmetric flow by nozzle clogging on inside-outside asymmetry. As expected, asymmetry between vortex formation frequency on inside and outside radius locations is not significant in these three cases. Minor differences are likely due to the limitations of the vortex formation frequency measurement method and a need for longer time averaging. Significantly more (26% more) vortices are observed on the left side for the small-clog case, and all vortices are formed to the left of the SEN with the severe-clog case. These vortices are caused by the velocity difference between the left and right side, which causes flow through the gap between the SEN and the mold, and vortex shedding on the downstream side. Furthermore, clogging increases vortex formation. Specifically, the total vortex frequency increases by 7% with the small-clog case and 62% with the severe-clog case relative to 8.2/minute with no clogging. Even with a non-clogged nozzle, many vortices are observed. These are due to random velocity variations between left and right sides, caused by turbulence in the mold.

Conclusions

- Nozzle clogging effects on nozzle and mold flow have been studied with three cases of clogging (no-clog, small-clog and severe-clog). The results are summarized in Figure 16.

Figure 16
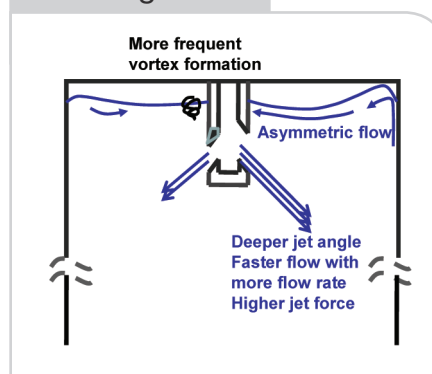
Phenomena in the mold with a clogged nozzle.

- Asymmetrical port size due to clogging causes asymmetric flowrate, velocity, turbulent kinetic energy, dissipation rate and jet force, resulting in asymmetric jet flow between sides.
- Increased, faster flow from the non-clogged nozzle port causes a deeper jet angle and higher force than from the clogged port, which causes asymmetric flow and an unbalanced double roll pattern in the mold.

- With severe clogging, the strong upward flow on the non-clogged side could shear liquid slag from the top surface, and the strong downward flow could penetrate inclusions deep into the mold cavity, causing internal defects.
- Surface flow always becomes slower and more chaotic toward the SEN, due to vortices forming in four regions near the SEN.
- With clogging, surface flow across the side with the non-clogged port is faster than with the clogged port. This stronger surface flow can cross the gap to suppress flow on the other side, and creates vortices.
- Vortices are caused by asymmetric flow between the right and left sides through the gap between the SEN and mold wide faces.
- More clogging causes more asymmetry of flow between the two sides.
- More clogging causes faster gap flow, and more vortices near the SEN on the side of the mold with the clogged port.
- The steady-state standard k-ε model shows a reasonable quantitative match with the measurements. This model overpredicts the asymmetric suppression of surface flow by the faster, non-clogged side. The limited accuracy of this steady-state model is perhaps due to complex transient vortexing flow. More accurate transient models, such as LES, are needed to improve model predictions.

Acknowledgments

References

1. Wolf, M.M., "History of Continuous Casting," *Steelmaking Conference Proceedings,* ISS, Warrendale, Pa., USA, 1992, pp. 83–137.

2. Thomas, B.G., and S.P. Vanka, "Study of Transient Flow Structures in the Continuous Casting of Steel," *NSF Design and Manufacturing Grantees Conference,* NSF, Washington, D.C., 2000.

3. Miki, Y., and S. Takeuchi, "Internal Defects of Continuous Casting Slabs Caused by Asymmetric Unbalanced Steel Flow in Mold," *ISIJ International,* Vol. 43, No. 10, 2003, pp. 1548–1555.

4. Zhang, L.F., et al., "Investigation of Fluid Flow and Steel Cleanliness in the Continuous Casting Strand," *Metallurgical and Materials Transactions B,* Vol. 38, No. 1, 2007, pp. 63–83.

5. Gupta, D.; S. Chakraborty; and A.K. Lahiri, "Asymmetry and Oscillation of the Fluid Flow Pattern in a Continuous Casting Mold: a Water Model Study," *ISIJ International,* Vol. 37, No. 7, 1997, pp. 654–658.

6. Chaudhary, R.; Lee, G-G.; Thomas B.G.; Cho, S-M.; Kim, S-H.; and Kwon, O-D., "Effect of Stopper-Rod Misalignment on Fluid Flow in Continuous Casting of Steel," *Metallurgical and Materials Transactions B,* Vol. 42, No. 2, 2011, pp. 300–315.

7. Li, B., and Tsukihashi, F., "Vortexing Flow Patterns in a Water Model of Slab Continuous Casting Mold," *ISIJ International,* Vol. 45, No. 1, 2005, pp. 30–36.

8. Kasai, N., and Iguchi, M., "Water Model Experiment on Melting Powder Trapping by Vortex in the Continuous Casting Mold," *ISIJ International,* Vol. 47, No. 7, 2007, pp. 982–987

9. Cho, S-M.; Lee, G-G.; Kim, S-H.; Chaudhary, R.; Kwon, O-D.; and Thomas, B.G., "Effect of Stopper Rod Misalignment on Asymmetric Flow and Vortex Formation in Steel Slab Casting," Jim Evans Honorary Symposium, *Proceedings of The Minerals, Metals, and Materials Society Annual Meeting 2009,* TMS, Vol. 139, 2009, pp. 71–77.

10. Hibbeler, L.C., and Thomas, B.G., "Investigation of Mold Flux Entrainment in CC Molds Due to Shear Layer Instability," *AISTech Conference and Exposition,* 2010.

11. Rackers, K.G., and Thomas, B.G., "Clogging in Continuous Casting Nozzles," *78th Steel Conference Proceedings,* ISS, Vol. 78, 1995, pp. 723–734.

12. Kemeny, F.L., "Tundish Nozzle Clogging — Measurement and Prevention," *McLean Symposium Proceedings,* ISS, 1998, pp. 103–110.

13. Thomas, B.G., and Bai, H., "Tundish Nozzle Clogging — Application of Computational Models," *18th Process Technology Division Conference Proceedings,* ISS, Vol. 18, 2001, pp. 895–912.

14. Bai, H., and Thomas, B.G., "Effects of Clogging, Argon Injection, and Continuous Casting Conditions on Flow and Air Aspiration in Submerged Entry Nozzles," *Metallurgical and Materials Transactions B,* Vol. 32B, 2001, pp. 707–722.

15. Zhang, L.; Wang, Y.; and Zuo, X., "Flow Transport and Inclusion Motion in Steel Continuous Casting Mold Under Submerged Entry Nozzle Clogging Condition," *Metallurgical and Materials Transactions B,* Vol. 39B, 2008, pp. 534–550.

16. Thomas, B.G., "Fluid Flow in the Mold," *Making, Shaping and Treating of Steel,* 11th ed., Vol. 5, Casting Volume, A. Cramb, ed., AIST, Warrendale, Pa., USA, 2003, pp. 14.1–14.41.

17. Thomas, B.G.; Huang, X.; and Sussman, R.C., "Simulation of Argon Gas Flow Effects in a Continuous Slab Caster," *Metallurgical and Materials Transactions B,* Vol. 25B, No. 4, 1994, pp. 527–547.

18. Thomas, B.G., and Zhang, L., "Review: Mathematical Modeling of Fluid Flow in Continuous Casting," *ISIJ International,* 2001, Vol. 41, No. 10, pp. 1181–1193.

19. Yuan, Q.; Sivaramakrishnan, S.; Vanka, S.P.; and Thomas, B.G., "Computational and Experimental Study of Turbulent Flow in a 0.4-Scale Water Model of a Continuous Steel Caster," *Metallurgical and Materials Transactions B,* Vol. 35B, 2004, pp. 967–982.

20. Ramírez-López, P.; Morales, R.D.; Sánchez-Pérez, R.; Demedices, L.G.; and Dávila, O., "Structure of Turbulent Flow in a Slab Mold," *Metallurgical and Materials Transactions B,* Vol. 36B, 2005, pp. 787–800. ✦

Nominate this paper

Did you find this article to be of significant relevance to the advancement of steel technology? If so, please consider nominating it for the AIST Hunt-Kelly Outstanding Paper Award at AIST.org/huntkelly.